Graduate School of Pure and Applied Sciences

Study on Whispering Gallery Mode Lasers of Self-Assembled Microspheres of Polymer-Lanthanide Metal Hybrids

(ランタノイド錯体–ポリマー複合体の自己組織化マイクロ球体からのウィスパリングギャラリーモードレーザーに関する研究)

Zakarias Seba Ngara

Doctoral Program in Material Sciences
Student ID number: 201630129
Doctor of Engineering
Advised by Professor Yohei Yamamoto

Summary

1. Introduction

Since the first laser was invented by Maiman in 1960,[1–3] the researches of laser microcavity to confine light are growing rapidly due to microlaser cavity provides strong optical confinement of light and greatly enhances light-mater interaction.[4] The discovery of laser cavity has a significant effect in the revolution of science and technology that benefits for human life, especially for medicine and telecommunications.[2] Optical laser microcavities are small device that confine light for long periods of time by repeated reflection.[5,6] According to the confinement of light, there are three kinds of laser maicrocavity. They are Fabry-Perot (F-P), Photonic crystal and whispering gallery mode (WGM) microcavities.[3,4,7] Among them, WGM microcavitiy possess the highest quality (*Q*)-factor.[8] The F-P microcavity as a conventional microresonator has low *Q*-factor due to low reflectivity of mirror and large size.[9] Thus, F-P microresonator is only suitable for one dimensional (1D) microresonator such as microfiber. In order to overcome the drawback of F-P microcavity, WGM microresonator was introduced. WGM microresonator have been demonstrated as excellent candidates for constructing low threshold and narrow linewidth lasers, low optical losses or high Q factor and miniature sizes due to small mode volume.[3] WGM resonance is one of the mechanisms to confine light inside microresonator when the light propagates along the circumference of the microresonator via total internal reflection (TIR).[10–12] The discovery of WGM microresonators gives a great significant role in optical modern microresonators because they have a small cavity with high *Q*-factor,[13] easy fabrications,[3,13,14] and high sensitivity,[12] so that they have significant application in area as diverse as cavity quantum electrodynamics (QED),[15] microlaser,[16,17] sensing,[18,19] nonlinear optic,[12,20] optical communications,[12] and other photonic devices. Since Garet, et.al.[21] demonstrated WGM lasing in the microsphere of CaF_2:Sm^{2+}, the research about WGM and its applications are growing rapidly. So far, WGM microresonators can be made from many kinds of material such as conjugated polymers (CPs),[11,18,22] organic dye polymer,[23–26] inorganic material,[21] lead halide perovskite material,[27] silica glass microsphere doped lanthanide (Ln) metal ion,[28–30] and other materials. There are some geometries of WGM microresonator including microdisk,[23] microring,[31,32] microsquare,[33,34] microsphere,[11,22,35] microhexagon,[36] microtaper,[3] and so forth.

At present, many researches about WGM resonators from self-assembly of dye doped polymers,[23–26] and CPs and/or blending CPs have been reported.[11,22,37–40] However, the investigation of WGMs resonance in the microresonators from the self-assembly between CP and/or polymer coordinated with Ln metal complex is very limited. To date, only one paper by Narayana, *et al.*,[41] demonstrated WGM photoluminescence (PL) inside polystyrene (PS) microspheres doped CP and terbium (III) complex. In this self-assembly, energy transfer (*ET*) occurs from Tb^{3+} ion to CP. As consequence, its WGM spectrum was in a broad spectral range

because the observed WGM (PL) is basically from CP. In 2018, Fernandez-Bravo *et al.*[19] fabricated PS microsphere coated thulium (Tm^{3+}) ion-doped sodium yttrium fluoride ($NaYF_4$) nanoparticle and displayed upconversion WGM lasing. In this case, the observed lasing at 470 nm is produced by direct excitation of Tm^{3+} ion in the PS microsphere without *ET* processes.

In this my work, WGM lasing will be demonstrated in the microsphere from the self-assembly between polymer containing alternating fluorene-terpyridine moieties and Ln complex where *ET* takes place from polymer to Ln^{3+} ion. As a result, it is to be expected that WGM PL is narrow and sharp band emission which is the characteristic of emission of the Ln^{3+} ion. The narrow and sharp emission of Ln^{3+} ion via *ET* is very important for application in laser and sensing. To achieve this purposes, poly[(9,9'-dioctyl-9H-fluoren-2,7-yl)-5,5'-(2,2':6',2"-terpyridine (F8tpy) as polymer which acts as a donor and europium thenoyltrifluoroacetonate trihydrate ($Eu(tta)_3.3H_2O$) as Ln metal complex which acts as an acceptor were selected and to be expected that WGM PL with narrow and sharp emission inside microcavity of F8tpy-Eu can be displayed via *ET* from F8tpy to europium (III) ion, Eu^{3+} ion. The choice of F8tpy is due to containing polyfluorene (PF) moiety which emits blue emission color and terpyridine (tpy) moiety which possess three nitrogen atoms that would be expected to bind Ln^{3+} ion[42] including Eu^{3+} ion. Whereas the choice of Eu^{3+} ion is due to it emits red emission color, narrow and sharp emission at around 610-625 nm, long lifetime,[43,44] and it has excellent color purity and chemical environment stability.[42] Thus, thenoyltrifluoroacetonate (tta) as ancillary ligand was selected because it can sensitize Eu^{3+} ion emission.[45] The molecular structure of F8tpy (a),[43] europium complex (b) and their complex, F8tpy-Eu (c) was displayed in Figure 1.

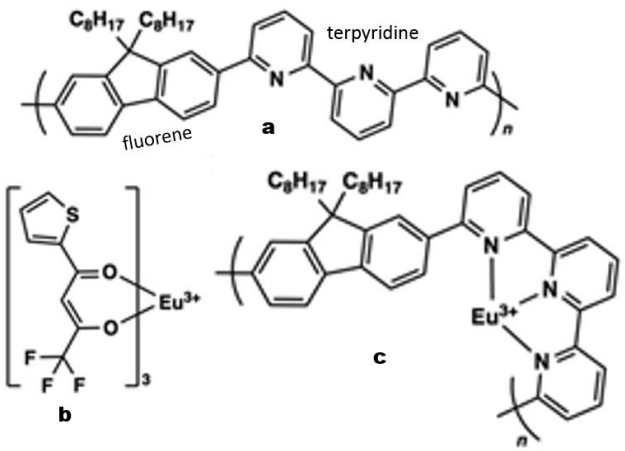

Figure 1. Molecular structures of F8tpy (**a**), $Eu(tta)_3$ (**b**), and F8tpy–Eu (**c**)

The self-assembly of F8tpy was prepared by vapor diffusion method.[11,46] Whereas the self-assembly of F8tpy-Eu was carried out by mini emulsion method.[18,47] Upon focuses laser, a single microsphere of F8tpy-Eu demonstrates WGM lasing with narrow and sharp emission at the red-color region, indicating that *ET* takes place efficiently from F8tpy to Eu^{3+} ion. The narrow and sharp band emission in the microsphere of F8tpy-Eu can be utilized for development of microlaser, chemical and bio-sensing, optical fiber, and other photonic devices. Therefore, the main objectives in my research is to fabricate microsphere from the self-assembly of F8tpy-Eu and to display WGM lasing resonance in the microsphere of F8tpy-Eu where *ET* takes place from F8tpy to Eu^{3+} ion.

Thus, in this work, the switching of WGM resonance will be displayed in the protonated and deprotonated microsphere of F8tpy. In the protonated microsphere of F8tpy, WGM resonance peak shifted to longer wavelength at 480-520 nm in comparison with WGM resonance peak of pristine microsphere of F8tpy at 420-440 nm. While in the deprotonated microsphere of F8tpy, WGM resonance peak is almost the same in the original microsphere of F8tpy. This indicates that the reversibility of WGM resonance takes place. The remarkable shift of WGM resonance peak in the microsphere of F8tpy indicated that F8tpy materials has a great potential candidate for applications in sensing and other photonic devices.

2. Experiments

2.1 Synthesis procedures of F8tpy using europium complex

The main materials, F8tpy and $[Eu(tta)_3].3H_2O$, were purchased from ADS Inc. and Aldrich Co Ltd., respectively. The other materials were purchased from Aldrich Co Ltd. without further purification. Synthesis process of F8tpy with europium complex was followed according to reference[48] with a small modification. The complex compound of F8tpy-Eu was obtained by blending equimolar amounts of F8tpy (10 mg, 0.0016 mmol) and europium complex (13.9 mg, 0.0016 mmol) in dry tetrahydrofuran solution (THF, 10 mL) under N_2 in two neck round-bottomed-

flask. After three cycles of vacuum and nitrogen gas, 10 mL of dry THF were added in two neck round bottomed flask and stirring for 24 h at 50 °C. After stirring process, the solvent was removed by evaporation. The crude product was washed with MeOH and was collected by filtration and dried in vacuum to yield F8tpy-Eu as yellow powder which is display in Figure 1. FTIR spectrum: 3114, 2950, 2878 (C-H), 2360 (C ≡ C), 1600 (C=O), 1539, 1531 (C=C), 1439, 1411, 1317, 1298, 1281, 1180, 1123, 1107, 1059, 932, 859, 787, 715, 678, 640, 583.

2.2 Absorbance and photoluminescence spectra measurement of F8tpy and F8tpy-Eu

F8tpy solution (50 µL, 3.2 x 10^{-3} M, $CHCl_3$) was drop casted onto a clean quartz substrate in air dried and analysed by using JASCO model UV-570 spectrophotometer and model FP-6200 spectrofluorometer, respectively. A similar procedure was followed for F8tpy-Eu, F8tpy-CSA and F8tpy-CSA-NaOH material.

2.3 Preparation of microspheres

2.3.1 Microsphere preparation of F8tpy

The microsphere of F8tpy was fabricated by using vapour diffusion (VD) method.[11,46,47] A 5-mL vial containing $CHCl_3$ solution of F8tpy (1.0 mg mL^{-1}, 2.0 mL) was put in a 50-mL vial containing 5 mL of MeOH. The smaller vial was still opened when it was placed in a bigger vial and the outer of bigger vial was capped and kept for 3 days in a thermostat bath at 25 °C. When MeOH vapor was slowly diffused into the $CHCl_3$ solution of F8tpy, yielding white precipitates.

2.3.2 Microsphere preparation of F8tpy-Eu

The microsphere of F8tpy-Eu was formed by mini emulsion (ME) method[18,47] and self-organized precipitation (SORP) methods.[41,49] For ME method, F8tpy-Eu was dissolved in $CHCl_3$ (10 mg mL^{-1}, 300 µL) then was added to an aqueous solution of sodium *n*-dodecyl sulfate (SDS, 1.0 x 10^{-2} M, 0.5 mL), and water (2 mL). This resultant solution was emulsified by vigorously stirring with homogenizer (30,000 rpm, 2 min) and kept for 3 days at 25 °C in an atmosphere to naturally evaporate $CHCl_3$. The excess SDS was removed by exchanging the supernatant water through centrifugation by three times. For SORP method, A THF solution of F8tpy-Eu (1mg/mL, 0.1 mL) was added in THF solution of polystyrene (5 mg/mL, 4 mL). Then, water (1 mL) was added in this mixture solution and kept it at least 1h to evaporate THF, resulting of precipitation

2.4 Preparation of protonated and deprotonated microsphere F8tpy using dipping method

For protonated microsphere of F8tpy, F8tpy suspension was drop-casted on a clean quartz and SiO_2 substrates, respectively and air-dried. Then these substrates containing microsphere of F8tpy were dipped in CSA solution (1 mg.mL^{-1}, MeOH, 3 mL) and kept for 2 days to evaporate MeOH. For deprotonated microsphere of F8tpy, the substrates containing protonated microsphere of F8tpy was dipped in NaOH solution (1 mg.mL^{-1}, MeOH, 3 mL) and kept for 2 days to evaporate MeOH.

2.5 Fluorescence, scanning electronic microscopic (SEM) micrographs

For fluorescence micrograph, the precipitation containing microsphere was drop-casted onto a clean quartz substrate and air-dried to immobilize microsphere on the substrate. Then, it was investigated by fluorescence microscope using an Olympus model BX53 Upright Microscope with excitation wavelength at 350-390 nm. For SEM micrograph, the suspension was drop-casted onto a clean SiO_2 substrate and air-dried to immobilize microsphere on the substrate. Then, it was carried out by Hitachi model SU-8000 FE-SEM operating at 10 kV. Silicon was used as a substrate and Au for coating.

2.6 Measurement of µ-PL spectrum

Precipitation of F8tpy, F8tpy-Eu, F8tpy-Eu:PS, F8tpy-CSA, and F8tpy-CSA-NaOH, respectively, were drop-casted onto a clean quartz substrate and air-dried to immobilize microsphere on the substrate. The µ-PL measurements were carried out with home-made µ-PL measurement system. A 355-nm pulsed laser (CNI model MPL-F-355-10mW-10%, pulse duration 7 ns, frequency 1 kHz) was passed through x100 objective lens (NA = 0.9) set on an optical microscope (Nicon model Eclipse LD100D) and excites a single microsphere of F8tpy, F8tpy-Eu and F8tpy-Eu:PS, respectively. The PL from a single microsphere was detected by a spectrometer (Lambda Vision model LV-MC3/T, grating: 300 grooves mm^{-1}) through an optical fiber.

3 Results and discussion

3.1 Absorption and photoluminescence spectra of F8tpy and F8tpy-Eu^{3+}

Figure 2 shows absorption and PL spectra at room temperature, of F8tpy and F8tpy-Eu.[50] The maxima absorption of F8tpy was observed at 347 nm which are attributed to the singlet–singlet absorption of polyfluorene and tpy moieties.[42] This peak is characterized by the π → π* transition of the fluorene[51] and tpy. In contrast, after F8tpy coordinated with Eu^{3+} ion, the absorption spectrum is slightly shifted and broaden to longer wavelength with maxima absorption at 350 nm indicating interaction between F8tpy and europium complex takes place.[42] As displayed in Figure 2a, inset, the color of F8tpy before and after coordinated with Eu^{3+} ion is white and yellow colour. By irradiation of UV light at wavelength of 365 nm, F8tpy and F8tpy-Eu emit blue and red colour emission, respectively (inset Fig.2b). The change of this color demonstrates that *ET* takes place from F8tpy to Eu^{3+} ion via tta.

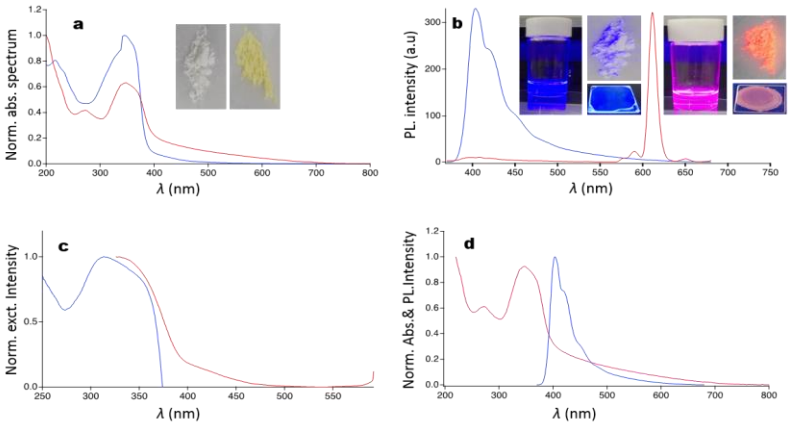

Figure 2 (a) Absorption (abs) spectra of cast films from F8tpy (blue) and F8tpy-Eu (red). Insets show photographs of powder samples of F8tpy (left) and F8tpy-Eu (right). (b) PL spectra of cast films from F8tpy (blue) and F8tpy-Eu (red). λ_{ex} = 350 nm. Insets show photographs of solutions, powders, and cast films of F8tpy (left) and F8tpy-Eu (right) under UV irradiation at 365 nm. (c) Normalized excitation spectra of cast films of F8tpy (blue, λ_{em} = 404 nm) and F8tpy-Eu (red, λ_{em} = 612 nm). (d) Normalized and overlap between PL spectrum of F8tpy (blue) and abs spectrum of F8tpy-Eu (red).

According to Figure 2b, by direct excitation at 350 nm, F8tpy emits in the range 370-680 nm but its intensity in the range from 550 to 680 nm is very weak. When F8tpy coordinated with Eu^{3+} ion and by direct excitation at 350 nm, the PL spectrum of F8tpy-Eu exhibits narrow and sharp peak with highest intensity at 612 nm ($^5D_0 \rightarrow {}^7F_2$ transition) which is the characteristic of Eu^{3+} ion. The other peaks appear at 577, 593, and 650 nm corresponding to $^5D_0 \rightarrow {}^7F_J$ (J = 0, 1, 3) transitions. The appearance of these peaks indicates that *ET* occurs from F8tpy to Eu^{3+} ion via tta. To confirm *ET* takes place from F8tpy to Eu^{3+}ion, excitation spectra of F8tpy and F8tpy-Eu were measured by monitoring PL at 404 nm for F8tpy and 612 nm for F8tpy-Eu where absorption bands at 314 nm and 350 nm for F8tpy and F8tpy-Eu, respectively (Figure 2c),[50] correspond well with their absorption spectra (Figure 2a). Thus, these results were consistent with the spectral overlap between of the emission spectrum of F8tpy and abs spectrum of F8tpy-Eu (**Figure 2d**). According to Figure 2b, the efficiency (η) of ET from F8tpy to Eu^{3+} ion is evaluated to be 0.90, using the following equation, $\eta_{DA} = 1 - (I_{DA}/I_D)$ where I_{DA} and I_D are the PL intensity with and without energy acceptor, respectively.[52]

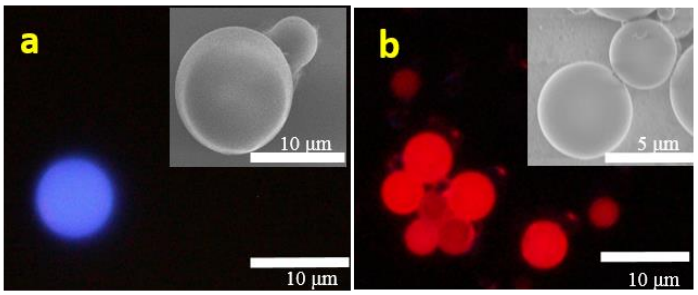

Figure 3 Fluorescent micrographs of microspheres from F8tpy (a) and F8tpy-Eu (b). λ_x = 350–390 nm. Insets show SEM micrographs of the microspheres.

3.2 Microspheres of F8tpy and F8tpy-Eu

Figure 3 shows fluorescence micrographs of microsphere of F8tpy (a) and F8tpy-Eu (b)[50]. Insets demonstrates SEM micrographs of microspheres. From fluorescence micrographs, upon photoexcitationn at 350-390 nm, the microspheres of F8tpy and F8tpy-Eu emit blue and red-color emission, respectively. From SEM micrographs, F8tpy and F8tpy-Eu form microsphere with well-defined and smooth surface with their average diameter (d_{av}) and standard deviation (σ) are

evaluated as 4.54 ± 2.14 and 3.17 ± 1.12 μm, respectively. F8tpy and F8tpy-Eu form microsphere because they have amorphous structure.

3.3 Whispering gallery mode spectrum of F8tpy and F8tpy-Eu

Figure 4a demonstrated WGM spectra of F8tpy (blue) and F8tpy-Eu (other colors).[50] Upon photoexcitation with focused laser (λ = 355 nm), a single microsphere of F8tpy displays WGM PL at a wide spectral range from 420 to 680 nm (Figure 4a, blue). This WGM PL consists of sharp and periodic lines which are attributed to transverse electric (TE) and magnetic (TM) modes as exhibited in Figure 5a. In contrast, a single microsphere of F8tpy-Eu, upon photoexcitation with focused laser at 355 nm, demonstrates WGM resonance in a narrow spectral range at 615–630 nm (Figure 4a red, yellow, and green). The narrow and sharp WGM peaks at 615-630 nm indicated that *ET* takes place from F8tpy to Eu^{3+} in the microsphere cavities of F8tpy-Eu. Thus, the number of WGM modes enhanced as increasing the diameter (d) of microsphere[53] of F8tpy-Eu from 3.24 to 4.86 μm. As displayed in Figure 4b, the intensity of WGM lasing peak at 615 nm strongly increases nonlinearly as the increase of pumping power (P) of laser. The intensity dependence is fitted to a power law x^S where S is the slope of power-law fit in the log-log plot[19,34] as exhibited in Figure 5c and clearly show the threshold pumping energy at 1.85 mJ.cm^{-2}. Under threshold pumping energy, the PL spectra is dominated by broad spontaneous emission and very weak. In contrast, above threshold, WGM lasing spectrum with narrow, sharp and strong emission was realized which demonstrate lasing action plot[19,34] in the microspheres of F8tpy-Eu. From Figure 5c, the s_1 and s_2 values presenting linear and superlinear regions are evaluated as to be 0.93 ± 0.04 and 2.46 ± 0.34, respectively. The presence of superlinear region confirms the lasing action inside microsphere. Above P_{th}, line width of the WGM lasing peak at 615 nm becomes narrow from 1.8 to 1.1 nm (Figure 4d). The abrupt lowering of line width above threshold also confirmed the lasing action within microsphere.[34] The line width and threshold pumping energy decreases when d of microsphere increases as displayed in Figure 5e and Figure 5f, respectively. The decrease of these line width and threshold pumping energy are induced by the small leakage loss of light in the microsphere with large size.[23,31,40]

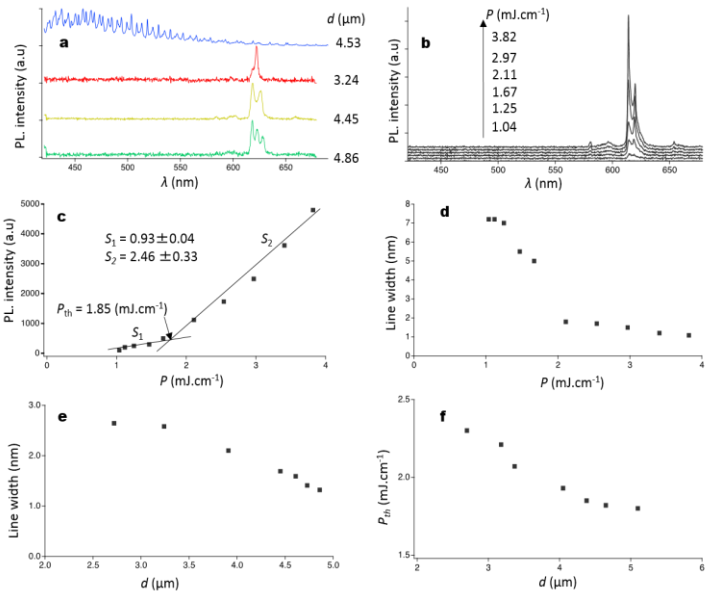

Figure 4 (a) WGM spectra of a single microsphere of F8tpy (blue) and F8tpy-Eu (red, yellow and green). (b) WGM lasing spectra of a single microsphere of F8tpy with d of 4.38 μm with P (mJ cm^{-2}). (c) Plot of the PL intensity at 615 nm versus P. (d) Plot of the line width of the PL peak at around 615 nm versus P. (e) Plot of line width of the peak at 615 nm versus d. f) Plot of P_{th} versus d.

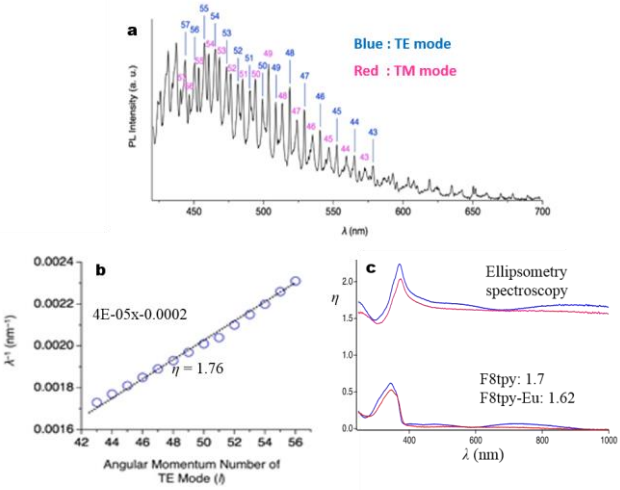

Figure 5 (a) Indices of TE (blue) and TM (pink) modes for the PL spectral lines of the F8tpy microsphere (d = 4.53 μm). (b) Plot of λ^{-1} versus the l of the TE mode. The dotted line indicates the linear fitting. (c) Wavelength dependency of the refractive indices for F8tpy (blue) and F8tpy-Eu (red) in cast films.

From WGM spectrum of F8tpy (Figure 5a), the refractive index (n) of F8tpy can calculated by plot λ^{-1} versus l (TE modes) based on the equation $\lambda^{-1} = (n\pi d)^{-1} l$ as demonstrated in Figure 5b. From this Figure, the n value of F8tpy is determined as 1.76 which is in reasonable agreement with ellipsometry spectroscopy measurement of 1.72 (Figure 5c).

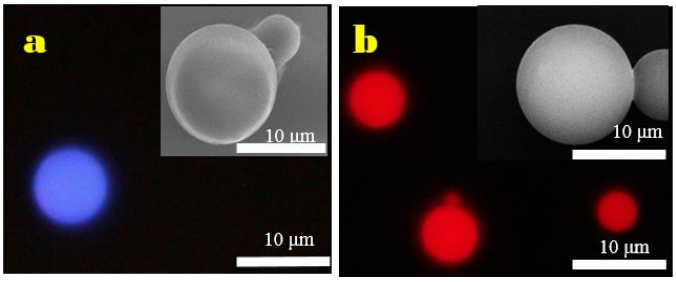

Figure 6 Fluorescent micrographs of microspheres from F8tpy (a) and F8tpy-Eu+PS (b). λ_x = 350–390 nm. Insets show SEM micrographs of the microspheres.

3.4 Microsphere of F8tpy-Eu + PS

The line width of WGM lasing peak at 615 nm in the microsphere of F8tpy-Eu, which was fabricated by ME method, is evaluated as 1.8 to 1.1 nm above threshold. This value is still large for lasing. One possible reason is the slight roughness of microsphere surface. Therefore, SORP method was adopted to fabricate F8tpy/Eu microsphere. In the SORP method, PS material is necessary to realize microsphere with well-defined and smooth. In this case, PS microsphere is only resonator[19,41] to generate WGM emission of F8tpy-Eu as a gain medium. PS material creates high-quality microsphere resonator because of its outstanding flexibility.[23] Figure 6b show fluorescence micrograph of microsphere of PS:F8tpy-Eu. From fluorescence micrograph, the microsphere of PS:F8tpy-Eu emit red-color emission indicating ET occurs from F8tpy to Eu^{3+} ion. From SEM image (Figure 6b, insets), the microsphere of PS:F8tpy-Eu with well-defined geometry and smooth surface which is smoother than that from ME method (Figure 3: inset). The value of the d_{av} and σ is 5.25 and 2.16 μm, respectively.

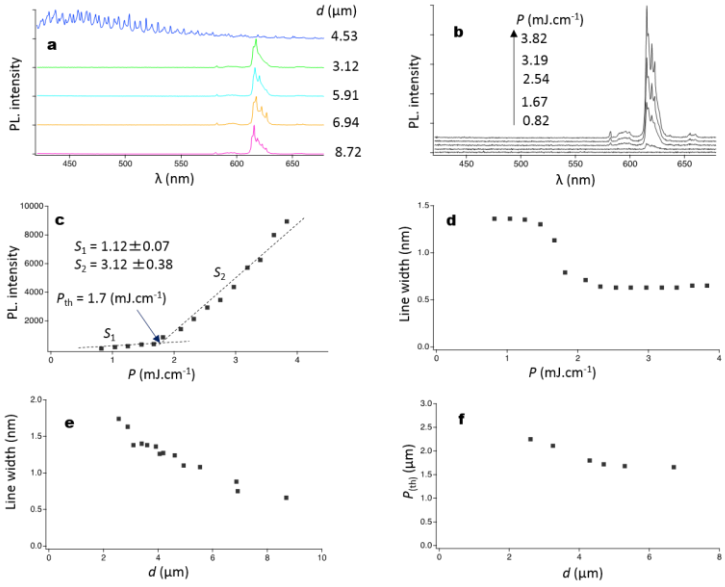

Figure 7 (a) WGM spectra of a single microsphere of F8tpy (blue) and F8tpy-Eu (Other color). (b) WGM lasing spectra of a single microsphere of F8tpy with d of 5.13 μm with P (mJ cm^{-2}). (c) Plot of the PL intensity at 615.481 nm versus P. (d) Plot of the line width of the PL peak at around 615 nm versus P. (e) Plot of line width of the peak at 615.481 nm versus d. f) Plot of P_{th} versus d.

3.5 Whispering gallery mode lasing in the microsphere of PS:F8tpy-Eu

Upon focused laser excitation at 355 nm, a single microsphere of F8tpy-Eu+PS demonstrated WGM resonance in the range of 615-630 nm which is the characteristic of Eu^{3+}ion as demonstrated in Figure 7a (green, gray, yellow and red with various d). When d of microsphere increases, the number of mode peak increases[53] which is in reasonable agreement with fundamental equation of WGM, $\pi\eta d = l\lambda$.[11] The appearance of WGM

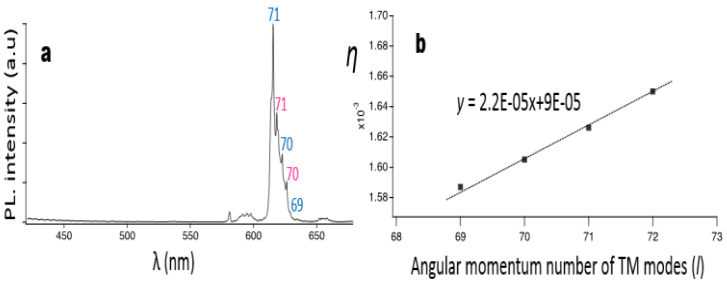

Figure 8 (a) Indices of TE (blue) and TM (pink) modes for the PL spectral lines of the microsphere of **F8tpy** (d = 8.72 μm). (b) Plot of λ^{-1} versus the l of the TE mode. The dotted line indicates the linear fitting.

resonance in range of 615-630 nm indicated *ET* takes place from F8tpy to Eu^{3+} ion. Figure 7b exhibited the nonlinear increase of intensity as increase the pumping power (*P*) of laser. The intensity dependence is fitted to a power law x^S where *S* is the slope of power-law fit in the log-log plot[19,34] as exhibited in Figure 8c and clearly show the threshold pumping energy at 1.7 $mJ.cm^{-2}$.

From Figure 7c, the s_1 and s_2 values corresponding with linear and the superlinear regions are estimated as to be 1.12 ± 0.07 and 3.12 ± 0.38, respectively. Above P_{th}, the line width of the WGM lasing peak becomes narrow from 1.0 to 0.6 nm (Figure 7d) which is smaller than previous result.[50] These values indicated that microsphere of PS:F8tpy-Eu has great potential for development of microlaser and sensing devices. Line width and threshold pumping power decreases as increasing the *d* of microsphere (Figure 7e and f), which are induced by the small leakage loss of light in the microsphere with large size.[31,40] From WGM spectrum of PS: F8tpy-Eu (Figure 8a) with its *d* of 8.72 µm, the refractive index (*n*) of PS:F8tpy-Eu can be calculated by plot λ^{-1} versus *l* (TE modes) based on the equation $\lambda^{-1} = (n\pi d)^{-1} l$ as demonstrated in Figure 8b. The *n* value of F8tpy-Eu is determined to be 1.67 which is agreement with ellipsometry spectroscopy measurement of 1.56. While the *n* value of F8tpy-Eu in thin film without PS is 1.62 (Figure 5c, red).

3.6 Protonated and deprotonated microsphere of F8tpy

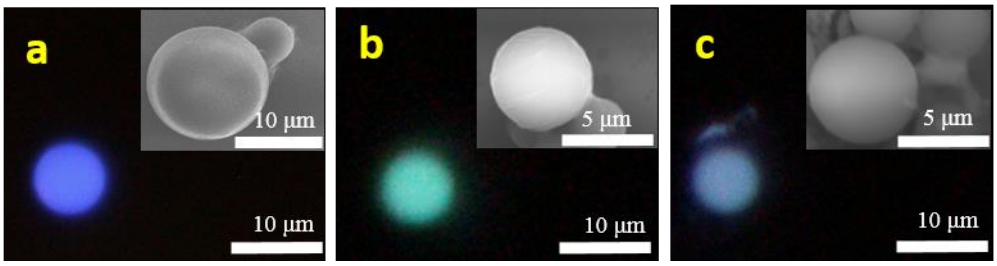

Figure 9 Fluorescent micrographs of microspheres from F8tpy (a)[50], protonated F8tpy (b) and deprotonated F8tpy (c). λ_{ex} = 350–390 nm. Insets show SEM micrographs of the microspheres

The protonated and deprotonated microsphere of F8tpy were prepared by diping method. Figure 9 shows Fluorescence micrographs of microspheres from pristine (a), protonated (b) and deprotonated of F8tpy. Insets demonstrate SEM micrographs of microspheres. From fluorescence micrographs, the microsphere of F8tpy clearly demonstrates switching of color from blue to green under protonated and from green to blue emission under deprotonated. Originally, microsphere of F8tpy emits blue-color emission (Figure 9a). After microsphere of F8tpy was dipped in CSA solution, the protonated microsphere of F8tpy emits green-color emission (Figure 9b), indicating microsphere of F8tpy was protonated by CSA. Furthermore, after protonated microsphere of F8tpy was dipped in NaOH solution, the deprotonated microsphere of F8tpy emits blue emission color (Figure 9c) which is almost the same with blue emission color of original microsphere of F8tpy (Figure 9a), indicating reversibility of emission color in the microsphere of F8tpy occurs.

From SEM micrographs, the microsphere of pristine (a), protonated (b) and deprotonated (c) of F8tpy demonstrates well-defined geometry. However, the surface of protonated and deprotonated microsphere of F8tpy is slightly rough in comparison with the surface of original microsphere of F8tpy. One possible reason is when the microsphere of F8tpy was dipped in CSA solution, during the evaporation of MeOH, precipitation of CSA is formed and distribution of CSA particles on the microsphere surface of F8tpy did not homogeneous and formed a few small fibers which originate from CSA due to crystal structure of CSA. Then, when the protonated microsphere of F8tpy was dipped in NaOH solution, CSA particles removed from surface of microsphere due to CSA dissolved in MeOH, then formed salt of sodium sulphite covered some parts of microsphere. According to the SEM micrographs, the value of d_{av} and σ of microsphere from native, protonated and deprotonated F8tpy are 4.54 and 2.14 µm, 4.6 and 1.88 µm, and 4.42 and 2.09 µm, respectively.

3.7 WGM resonance inside original, protonated and protonated microsphere of F8tpy

Figure 10 demonstrates the switching of WGM resonance inside protonated and deprotonated microsphere of F8tpy. Upon photoexcitation with focused laser at λ = 355 nm, a single original microsphere of F8tpy exhibits WGM emission with periodic lines at broad region from 420 to 680 nm with maxima WGM emission band around 420-440 nm (blue, d = 2.57 µm). In contrast, a single protonated microsphere of F8tpy, upon phoptoexcitation with focused laser at 355 nm, demonstrates WGM emission with periodic lines at a wide spectral range from 420 to 680 nm but maxima WGM emission band at around 480-520 nm (green, d = 2.66 µm). This maxima emission band region shifted to longer wavelength which is caused by protonation of F8tpy using CSA. Interestingly, a single deprotonated microsphere of F8tpy (blue, d = 2.63 µm) displays WGM emission in the range of 420-680 nm with maxima WGM emission band at around 420-440 nm which is almost the same with Maxima WGM emission of pristine microsphere of F8tpy. These results clearly demonstrates the switching of WGM resonance inside protonated and deprotonated microsphere of F8tpy. The remarkable switching of the WGM resonance inside microsphere of F8tpy exhibits that the microsphere of F8tpy can be applied for development of sensing device and other photonic devices.

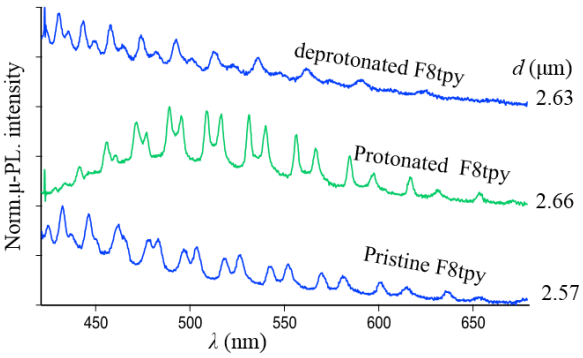

Figure 10 WGM spectra inside microsphere of pristine, protonated and deprotonated F8tpy

4. Conclusion

The microsphere of F8tpy was prepared by VD method. Whereas the microsphere of F8tpy-Eu was fabricated by ME and SORP methods. In the first research, the microspheres of F8tpy and F8tpy-Eu were prepared by using VD and ME methods, respectively. The microsphere of F8tpy and F8tpy-Eu emit blue and red-color emission with their d_{av} is 4.54 and 3.17 µm, respectively. Upon photoexcitation with focused laser at λ = 355 nm, a single microsphere of F8tpy demonstrates WGM resonance in the broad range from 420 to 680 nm. In contrast, a single microsphere of F8tpy-Eu, upon photoexcitation with focused laser at λ = 355 nm, displays WGM lasing with narrow and sharp emission at 615 nm which is the characteristic of the Eu^{3+} ion emission, indicating *ET* takes place in the microsphere from F8tpy to Eu^{3+} ion. From WGM lasing spectra, it clearly show threshold pump energy of 1.85 mJ.cm^{-1} with the line width of WGM lasing peak at 615 is 1.8 to 1.1 nm above threshold pump energy.

In the second research, the microsphere F8tpy-Eu was prepared by using SORP method. From SEM image, the microsphere of PS:F8tpy-Eu is well-defined and very smooth surface with d_{av} of 5.26 µm. The microsphere of PS:F8tpy-Eu emits red-color emission which originated from Eu^{3+} ion via *ET* from F8tpy to Eu^{3+} ion. Upon focuses laser of 355 nm, a single microsphere of PS:F8tpy-Eu shows WGM lasing with narrow and sharp emission at 615 nm which is the characteristic of the Eu^{3+} ion. This peaks clearly confirmed that *ET* occurs in the microsphere from F8tpy to Eu^{3+} ion. The realized line width of WGM lasing peak is less than 1 nm, which is smaller than previous results (ME method). Thus, the obtained threshold pump energy of 1.7 mJ cm^{-1} is lower than previous result. The obtained narrow and sharp WGM lasing at around 614-630 nm in the microsphere of PS:F8tpy-Eu are to be expected to apply for development of microlaser devices, chemical and biological sensing, optic fibre, and other photonic devices with high performances

In the third research, the protonated and deprotonated microsphere of F8tpy were prepared by dipping method. From fluorescence micrograph, it clearly displays the color switching of F8tpy microsphere under protonated and deprotonated process by using dipping method. Thus, switching of WGM resonance inside microsphere of F8tpy takes place under protonated and depronated process. Finally, the remarkable switching of the WGM resonance inside microsphere of F8tpy exhibits that the microsphere of F8tpy can be applied for development of sensing device and other photonic devices.

References

[1] T. H. Maiman, *Nature* **1960**, *187*, 493–494.
[2] I. D. W. Samuel, G. A. Turnbull, *Chem. Rev* **2007**, *107*, 1272–1295.
[3] L. He, S. K. Ozdemir, L. Yang, *Laser Photonic Rev.* **2013**, *82*, 60–82.
[4] V. D. Ta, S. Yang, Y. Wang, Y. Gao, T. He, R. Chen, H. V. Demir, H. Sun, *Appl. Phys. Lett.* **2015**, *107*, 1–5.
[5] E. P. Ostby, Photonic Whispering-Gallery Resonators in New Environments, **2009**.
[6] G. A. Cohoon, Fabrication , Characterization , and Application of Microresonators and Resonant Structures, Arizona University, **2018**.
[7] I. Lamei, Kandas, Silica Microspheres Functionalized with Self-Assembled Nanomaterials, Virginia Polytechnic Institute and State University, **2012**.
[8] G. Lin, Fabrication and Characterization of Optical Microcavities Functionalized by Rare-Earth Oxide Nanocrystals：Realization of a Single-Mode Ultra Low Threshold Laser, Xiamen University, **2010**.
[9] V. Duong Ta, R. Chen, L. Ma, Y. Jun Ying, H. Dong Sun, *Laser Photonics Rev.* **2013**, *7*, 133–139.
[10] N. B. Tomazio, A. J. G. Otuka, G. F. B. Almeida, X. Rosello-Mecho, M. V. Andres, C. R. Mendonca, *J. Polym. Sci. Part B Polym. Phys.* **2017**, *55*, 569–574.
[11] K. Tabata, D. Braam, S. Kushida, L. Tong, J. Kuwabara, T. Kanbara, A. Beckel, A. Lorke, Y. Yamamoto, *Sci. Rep.* **2014**, *4*, 3–7.
[12] S. Ciftci, A. Mikosch, B. Haehnle, Ł. Witczak, A. J. C. Kuehne, *Chem. Commun.* **2016**, *52*, 14222–14225.
[13] T. Reynolds, N. Riesen, A. Meldrum, X. Fan, J. M. M. Hall, T. M. Monro, A. Franc, *Laser Photonic Rev.* **2017**, *11*, 1–20.
[14] Y. Yang, F. Lei, S. Kasumie, L. Hu, J. Ward, L. Yang, S. N. Chormaic, *Opt. Soc. Am.* **2016**, *1*, 1–7.
[15] and H. J. K. T. Aoki, B. Dayan, E. Wilcut, W. P. Bowen, A. S. Parkins, T. J. Kippenberg, K. J. Vahala, *Nature* **2006**, *443*, 671–674.
[16] V. D. Ta, S. Caixeiro, F. M. Fernandes, R. Sapienza, *Adv. Opt. Mater.* **2017**, *5*, 1–6.
[17] V. D. Ta, R. Chen, H. D. Sun, *Adv. Mater.* **2012**, *24*, OP60-OP64.
[18] M. Gao, C. Wei, X. Lin, Y. Liu, F. Hu, Y. S. Zhao, *Chem. Commun.* **2017**, *53*, 3102–3105.
[19] A. Fernandez-bravo, K. Yao, E. S. Barnard, N. J. Borys, E. S. Levy, B. Tian, C. A. Tajon, L. Moretti, M. V. Altoe, S. Aloni, et al., *Nat. Nanotechnol.* **2018**, *13*, 572–577.
[20] D. V Strekalov, C. Marquardt, A. B. Matsko, *J. Opt.* **2016**, *18*, 123002.
[21] W. L. Garrett, C. G. B., Kaiser, W., and Bond, *Phys. Rev.* **1961**, *124*, 1807–1809.
[22] S. Kushida, D. Braam, C. Pan, T. D. Dao, K. Tabata, K. Sugiyasu, M. Takeuchi, S. Ishii, T. Nagao, A. Lorke, et al., *Macromolecules* **2015**, *48*, 3928–3933.
[23] C. Wei, S. Y. Liu, C. L. Zou, Y. Liu, J. Yao, Y. S. Zhao, *J. Am. Chem. Soc.* **2015**, *137*, 62–65.
[24] Q. Lu, X. CHen, Sh. Xie, X. Wu, *Opt. Express* **2018**, *26*, 20183–20191.
[25] A. François, N. Riesen, H. Ji, S. A. V, T. M. Monro, *Appl. Phys. Lett. X* **2015**, *106*, 1–4.
[26] A. François, N. Riesen, K. Gardner, T. M. Monro, A. Meldrum, *Opt. Express* **2016**, *24*, 12466–12477.
[27] N. Kurahashi, V. Nguyen, F. Sasaki, H. Yanagi, *Appl. Phys. Lett.* **2018**, *011107*, 1–6.
[28] K. Miura, K. Tanaka, K. Hirao, *J. Mater. Sci. Lett.* **1996**, *15*, 1854–1857.
[29] V. Sandoghdar, F. Treussart, J. Hare, V. Lefèvre-Seguin, J. M. Raimond, S. Haroche, *Phys. Rev. A* **1996**, *54*, R1777–R1780.
[30] Z. P. Cai, H. Y. Xu, G. M. Stéphan, P. Féron, M. Mortier, *Opt. Commun.* **2004**, *229*, 311–315.
[31] C. Zhang, C. Zou, Y. Yan, C. Wei, J. Cui, F. Sun, J. Yao, Y. S. Zhao, *Adv. Opt. Mater.* **2013**, *1*, 357–361.
[32] C. Zhang, C.-L. Zou, Y. Zhao, C.-H. Dong, C. Wei, H. Wang, Y. Liu, G.-C. Guo, J. Yao, Y. S. Zhao, *Sci. Adv.* **2015**, *8*, 1–7.
[33] Y. S. . Zhang, Wei; Yao, Jiannian, and Zhao, *Acc. Chem. Res.* **2016**, *49*, 1691−1700.

[34] X. Wang, Q. Liao, X. Lu, H. Li, Z. Xu, H. Fu, *Sci. Rep.* **2014**, *4*, 1–8.
[35] M. Jiao, N. Guo, W. Lü, Y. Jia, W. Lv, Q. Zhao, B. Shao, H. You, *Dalt. Trans.* **2013**, *42*, 12395.
[36] X. Wang, Q. Liao, Q. Kong, Y. Zhang, Z. Xu, X. Lu, H. Fu, *Angew. Chem.* **2014**, *126*, 5973–5977.
[37] H. Dong, C. Zhang, X. Lin, Z. Zhou, J. Yao, Y. S. Zhao, *Nano Lett.* **2017**, *17*, 91–96.
[38] W. Zhang, J. Yao, Y. S. Zhao, *Acc. Chem. Res.* **2016**, *49*, 1691–1700.
[39] S. Kushida, S. Okabe, T. D. Dao, S. Ishii, T. Nagao, A. Saeki, M. Kijima, Y. Yamamoto, *RSC Adv.* **2016**, *6*, 52854–52857.
[40] X. Wang, Q. Liao, Q. Kong, Y. Zhang, Z. Xu, X. Lu, H. Fu, *Angew. Chemie - Int. Ed.* **2014**, *53*, 5863–5867.
[41] Y. S. L. V. Narayana, D. Venkatakrishnarao, A. Biswas, M. A. Mohiddon, N. Viswanathan, R. Chandrasekar, *ACS Appl. Mater. Interfaces* **2016**, *8*, 952–958.
[42] C. Yang, J. Xu, Y. Zhang, Y. Li, J. Zheng, L. Liang, M. Lu, *J. Mater. Chem. C* **2013**, *1*, 4885–4901.
[43] D. A. Turchetti, M. M. Nolasco, D. Szczerbowski, L. D. Carlos, L. C. Akcelrud, *Phys. Chem. Chem. Phys.* **2015**, *17*, 26238–26248.
[44] A. K. Singh, S. K. Singh, H. Mishra, R. Prakash, S. B. Rai, *J. Physc. Chem. B* **2010**, *114*, 13042–13051.
[45] M. D. McGehee, T. Bergstedt, C. Zhang, A. P. Saab, M. B. O'Regan, G. C. Bazan, V. I. Srdanov, A. J. Heeger, *Adv. Mater.* **1999**, *11*, 1349–1354.
[46] T. Adachi, L. Tong, J. Kuwabara, T. Kanbara, A. Saeki, S. Seki, Y. Yamamoto, *J. AM. Chem. Soc.* **2013**, *135*, 870–876.
[47] Y. Yamamoto, D. Okada, S. Kushida, Z. S. Ngara, O. Oki, *J. Vis. Exp* **2017**, *124*, e55934.
[48] T. Yasuda, I. Yamaguchi, T. Yamamoto, *Adv. Mater.* **2003**, *15*, 293–296.
[49] H. Yabu, *Polym. J.* **2013**, *45*, 261–268.
[50] Z. S. Ngara, D. Okada, O. Oki, Y. Yamamoto, *Chem. Asian J.* **2018**, *X*, https://doi.org/10.1002/asia.201801219.
[51] H. Xu, J. Wang, Y. Wei, G. Xie, Q. Xue, Z. Deng, W. Huang, *J. mater. Chem C* **2015**, *3*, 1893–1903.
[52] D. J. Harkin, K. Broch, M. Schreck, H. Ceymann, A. Stoy, C. Yong, M. Nikolka, I. Mcculloch, N. Stingelin, C. Lambert, *Adv. Mater* **2016**, *28*, 6378–6385.
[53] Y. Wei, X. Lin, C. Wei, W. Zhang, Y. Yan, Y. S. Zhao, *ACS Nano* **2017**, *11*, 597–602.